Homework 4 - Field and Service Robot

Lisi Vittorio

16 giugno 2025

Matricola:P380000262

Istructions

Link github for matlab code:`https://github.com/vitlisi/HW4_Field.git`

Indice

1 Exercise 1

The buoyancy effect is a force resulting from the pressure exerted by the surrounding fluid (in this case, water) on a submerged body. It acts upward, in the opposite direction to gravity, and is equal to the weight of the volume of fluid displaced by the body.

In underwater robotics, the buoyancy effect is fundamental as it directly affects the robot's balance and stability. The buoyant force acts on the center of buoyancy, while the gravitational force acts on the center of mass. When these two points do not coincide, a torque is generated that can cause the vehicle to rotate. This has significant dynamic effects and must be taken into account both in the modeling and in the control design of the underwater robot.

In contrast, in aerial robotics, the buoyancy effect is generally neglected. Air has a much lower density than water, and the resulting Archimedes force is negligible compared to the weight of the vehicle itself. For this reason, in UAVs (Unmanned Aerial Vehicles), the buoyancy effect does not significantly affect the dynamic behavior of the system and can be ignored in the model equations.

2 Exercise 2

False. The effect of added mass represents the additional inertia that a body must overcome when accelerating in a fluid. This happens because the moving body must also displace the surrounding fluid, generating a reactive force. Although it is not a structural material load, from a dynamic perspective it behaves like an additional mass, significantly affecting the equations of motion of an underwater robot.

True. The effect of added mass is relevant in underwater robotics because the density of water is comparable to that of the vehicle. This means that the interaction with the fluid cannot be neglected, as the robot, when accelerating, sets in motion a portion of fluid that resists movement. This effect, however, is negligible in terrestrial or aerial robotics, where the fluid density is much lower than that of the body.

True. Damping forces, such as drag and viscous lift, act in the opposite direction to the relative velocity of the vehicle with respect to the fluid. These forces dissipate energy and have a stabilizing role in the system, contributing to the reduction of oscillations and convergence toward an equilibrium condition. For this reason, they are fundamental in the stability analysis of an underwater vehicle.

False. Ocean currents are modeled in the world frame, as they represent a property of the physical environment. It is incorrect to refer them directly to the robot's body frame, which is a non-inertial system. In simplified dynamic models, currents are often considered null or constant to reduce computational complexity. When included, the relative velocity between the vehicle and the current is calculated in the world frame, and then transformed into the body frame via inverse

rotation. Only this relative velocity is used to evaluate hydrodynamic forces such as damping and added mass.

3 Exercise 3

A comparative analysis was conducted across the six different gaits (`gait = 0--5`) of the quadruped robot, in order to evaluate their performance under significant parametric variations that directly affect system dynamics. The gaits, defined according to standard locomotion patterns inspired by biological and robotic schemes, are:

- **Gait 0 – Trot**: symmetric gait with alternating diagonal limb support.
- **Gait 1 – Bound**: dynamic gait with synchronized movement of front and rear legs.
- **Gait 2 – Pacing**: lateral pattern, with limbs on the same side moving in phase.
- **Gait 3 – Gallop**: highly dynamic gait with aerial phases.
- **Gait 4 – Trot Run**: accelerated version of the trot.
- **Gait 5 – Crawl**: quasi-static gait with three legs always in support.

During the analysis, four key parameters relevant to locomotion were varied:

- **Robot mass**: increased from 5.5 kg to **15 kg** to simulate high-load conditions;
- **Friction coefficient** (μ): reduced to **0.5** to simulate low-traction surfaces;
- **Desired speed** (`v_d`): increased up to **2.0 m/s** to test dynamic capabilities;
- **Yaw rotation and lateral displacement**: first a yaw rotation followed by a sideways motion at **0.5 m/s**.

For each gait–parameter combination, a full simulation was performed using Model Predictive Control (MPC) and solved via QP, analyzing trajectories, vertical contact forces (Fz), and overall dynamic performance.

Since the goal of this analysis is to identify, for each parameter scenario, the **most effective and robust solution**, the report presents only the **two best and one worst** cases for each type of variation (mass, friction, desired speed, yaw and lateral motion). Results were selected based on the following criteria:

- **Dynamic stability**: absence of tipping or slipping during locomotion;
- **Regularity of contact forces** (`Fz`): realistic and dynamically consistent distribution;
- **Tracking of desired speed**: robot's ability to effectively follow the imposed trajectory;
- **Control robustness**: stable response even under adverse conditions (high mass, low traction, high speed).

Selecting the best cases allows identifying the most suitable gait for each dynamic context, facilitating the integration of optimal locomotion patterns into an adaptive controller.

Results – Mass Variation

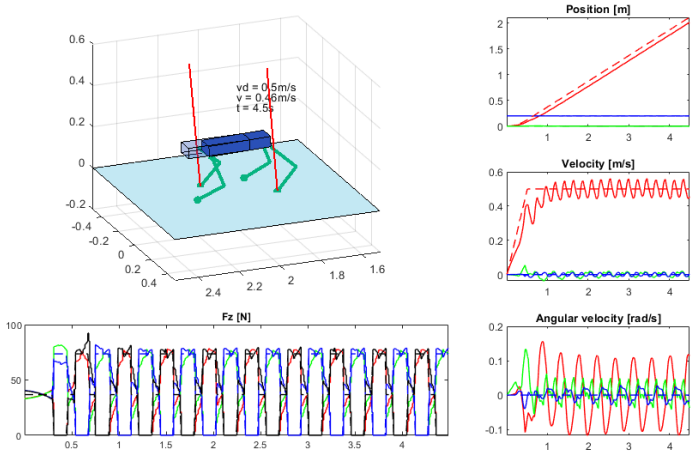

Figura 1: Gait 0 – Trot: shows stable behavior even with a mass of 15 kg. The diagonal alternation between front and hind legs ensures good load balance and regular distribution of vertical ground reaction forces. Oscillations remain limited and speed tracking is consistent.

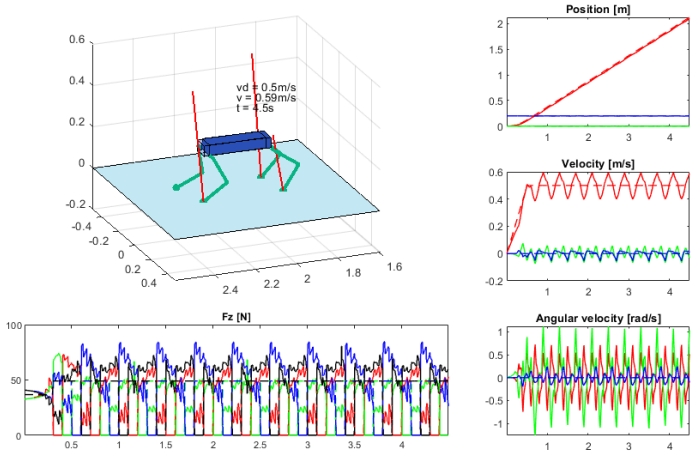

Figura 2: Gait 5 – Crawl: confirmed as **the most robust gait under heavy load**. The constant presence of three legs in support enables the system to maintain high stability, reducing inertial effects and ensuring continuous ground contact. Movement is slow but very safe.

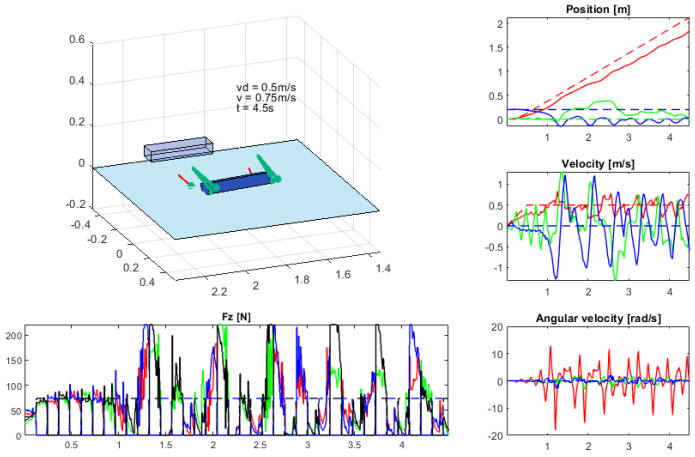

Figura 3: Gait 2 – Pacing: proves to be the **least stable configuration under heavy load**. The synchronized lateral movement of legs on the same side amplifies torque moments, leading to instability and excessive oscillations. Contact forces are unbalanced and the system quickly loses equilibrium.

Results – Friction Variation

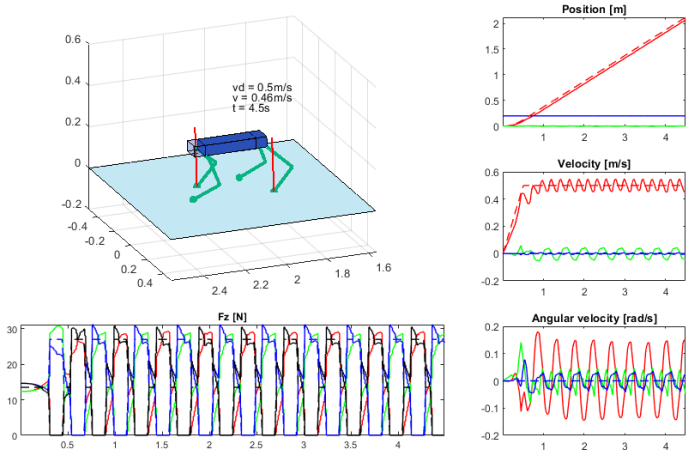

Figura 4: Gait 0 – Trot: maintains good stability even with a reduced friction coefficient of $\mu = 0.5$. The diagonal leg arrangement allows effective balance, though slight slipping is observed during swing phases. Speed tracking remains acceptable.

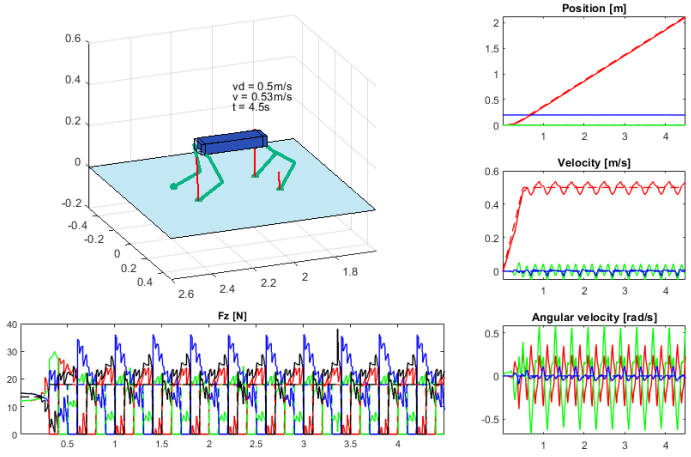

Figura 5: Gait 5 – Crawl: proves to be **the most stable under low traction**. The constant support from three legs strongly limits slipping and enables safe, steady locomotion even on slippery surfaces. The trade-off is lower forward speed.

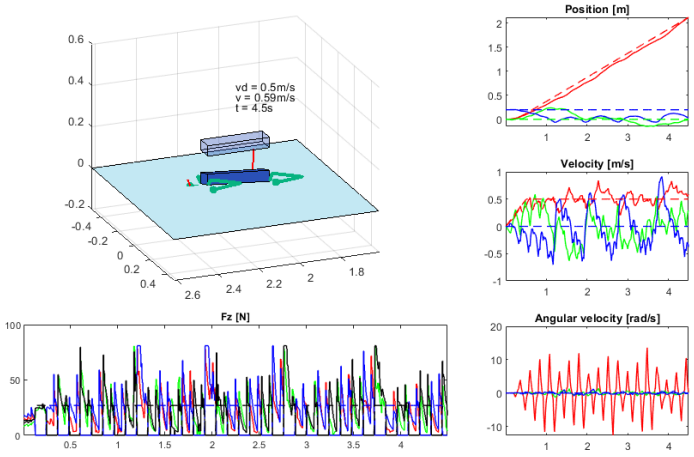

Figura 6: Gait 2 – Pacing: **unstable on low-traction surfaces**. The simultaneous movement of same-side legs creates high roll moments and reduces support effectiveness, causing slippage and loss of stability.

Results – Desired Speed Variation

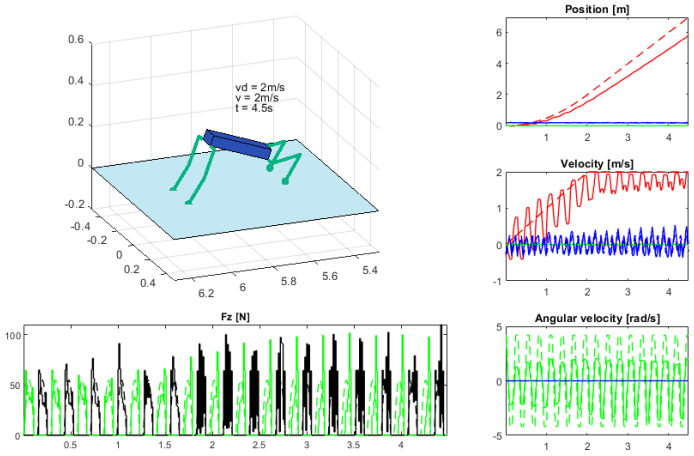

Figura 7: Gait 1 – Bound: shows good adaptability to high desired speeds (2 m/s). Its dynamic nature and aerial phase make this gait effective and stable in maintaining the target speed despite noticeable bouncing.

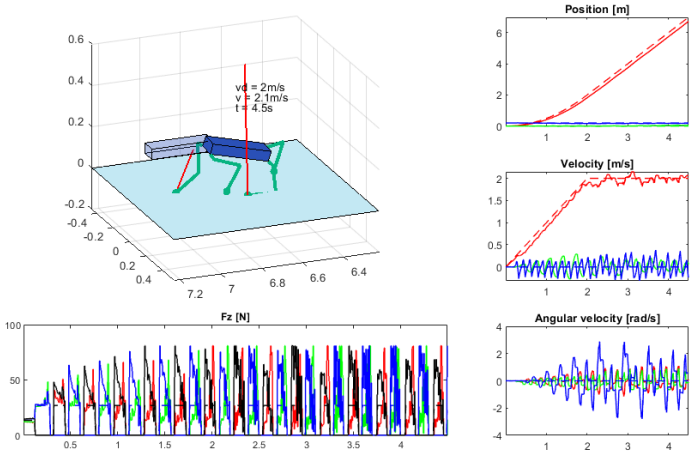

Figura 8: Gait 4 – Trot Run: used in place of gallop (Gait 3), which exhibited trajectory anomalies in simulation (undesired lateral movement). Trot run proves to be a **valid intermediate choice**, remaining stable even at sustained speeds.

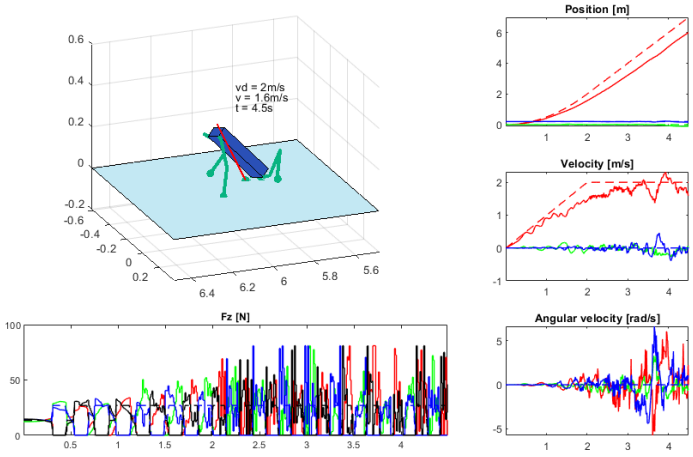

Figura 9: Gait 0 – Trot: **unstable at high speeds**. The absence of an aerial phase and reduced support base cause oscillations and loss of traction.

Results – Yaw and Lateral Displacement

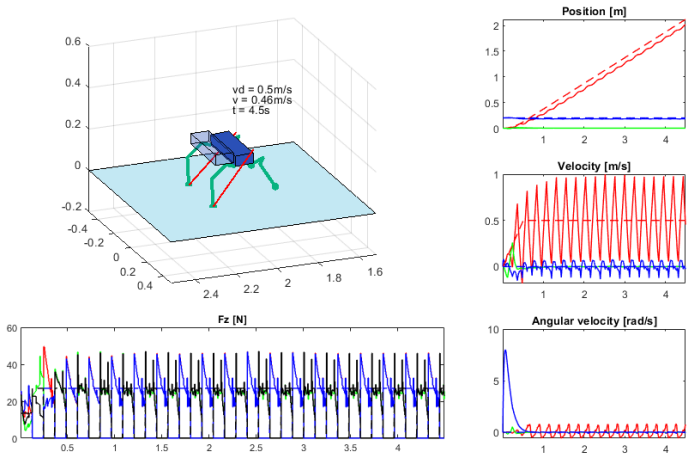

Figura 10: Gait 2 – Pacing: shows decent lateral maneuverability and rotation capability. Transverse movement is overall controlled, but roll moments are observed that require solid dynamic balancing.

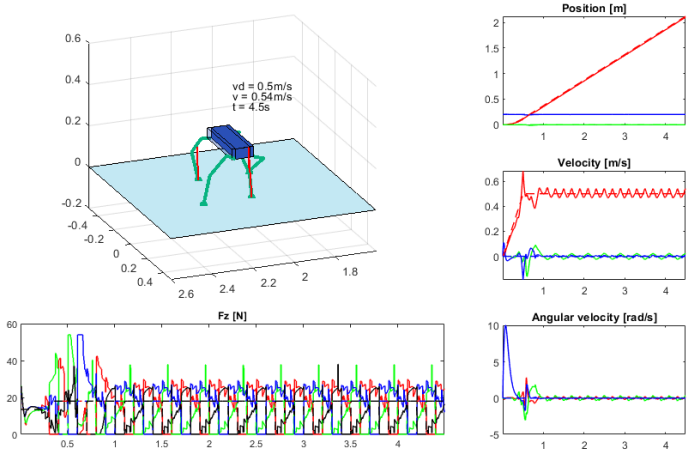

Figura 11: Gait 5 – Crawl: confirms its high stability even during complex maneuvers such as rotations and lateral displacements. The constant support of three legs ensures continuous balance, making it the most reliable for lateral control.

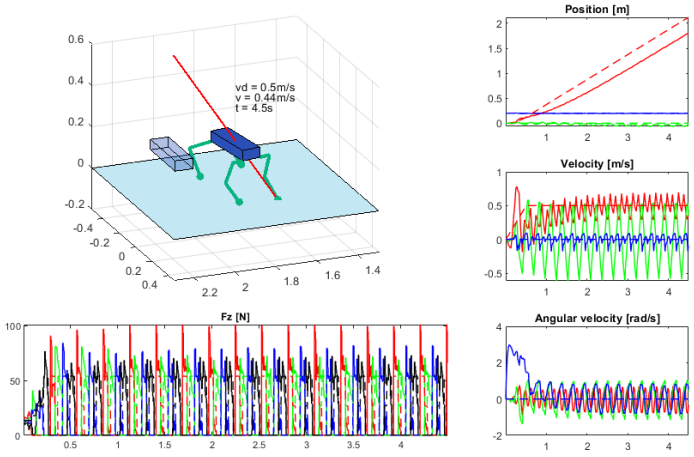

Figura 12: Gait 3 – Gallop: **unstable during lateral maneuvers**. High forces concentrated on a few legs during the aerial phase cause loss of grip and imbalance, compromising the effectiveness of rotation and lateral control.

Final Conclusions

The comparative analysis among the different gaits revealed that no gait is universally optimal; rather, performance varies significantly depending on dynamic and environmental conditions.

In particular, the **crawl gait (gait 5)** proved to be the most stable under high load or low traction, due to its high support factor. Conversely, the **bound gait (gait 1)** showed excellent performance at high speeds, while **trot (gait 0)** represents a good compromise for nominal scenarios. More dynamic gaits like **gallop (gait 3)** are effective only under very specific conditions but tend to lose stability in the presence of disturbances.

These results provide a solid foundation for future integration of an adaptive *gait selector* in real environments, capable of automatically modulating the gait based on the operational context.

4 Exercise 4

The objective of this simulation is to analyze the dynamic behavior of the rimless wheel under variations of the **initial angular velocity** $\dot{\theta}_0$, evaluating whether the system converges to a *stable limit cycle*.

Several initial angular velocity values, both positive and negative, were tested, including:

The three cases: $\dot{\theta}_0 = 0.95$ rad/s (standard), $\dot{\theta}_0 = 1.095$ rad/s, $\dot{\theta}_0 = -1.1$ rad/s

In the first case, it is observed that the system **fails to maintain cyclic motion**: the angular velocity quickly decreases and nullifies after a few impacts, bringing the system to a stop. This behavior is due to the initial kinetic energy being insufficient to overcome the slope of the incline (γ), thus the wheel enters a double support phase, during which the dynamics halt. The phase portrait confirms the absence of a limit cycle, showing a trajectory that converges to the origin.

In the second case, with $\dot{\theta}_0 = 1.095$ rad/s, the behavior is significantly different: the wheel manages to maintain continuous and regular oscillation. The time trajectories of $\theta(t)$ and $\dot{\theta}(t)$ show periodic behavior, and the phase portrait highlights the formation of a **closed and attractive limit cycle**, to which the system converges from various initial conditions.

In the third case, with $\dot{\theta}_0 = -1.1$ rad/s, the system stops quickly after a few impacts, similar to the first case. Although one might expect a mirrored behavior compared to the positive case, the presence of the slope ($\gamma > 0$) breaks this symmetry: gravity, instead of helping the motion, hinders it, favoring energy loss. The phase portrait confirms the absence of a limit cycle, showing a trajectory that converges to the origin.

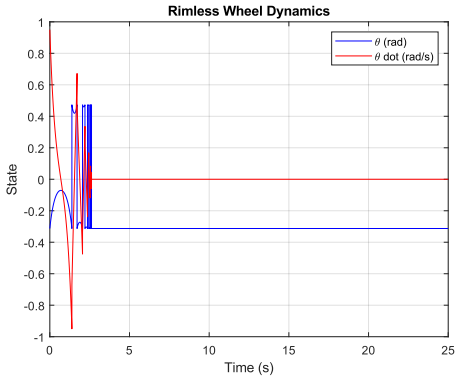

Figura 13: Time evolution for $\dot{\theta}_0 = 0.95$. The system stops after a few impacts: angular velocity quickly nullifies.

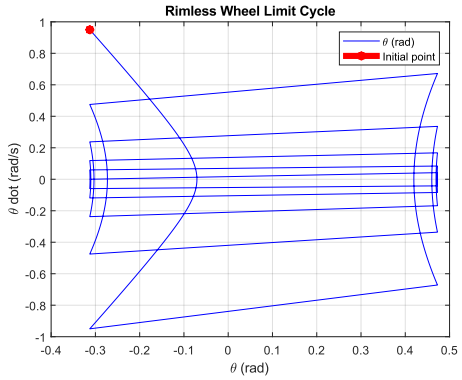

Figura 14: Phase portrait for $\dot{\theta}_0 = 0.95$. The trajectory converges to the origin, indicating the absence of a limit cycle.

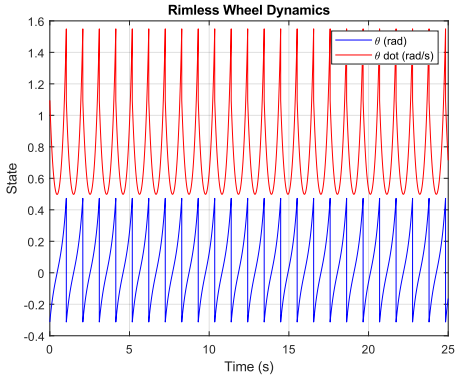

Figura 15: Time evolution for $\dot{\theta}_0 = 1.095$. The system enters a stable and persistent cyclic motion.

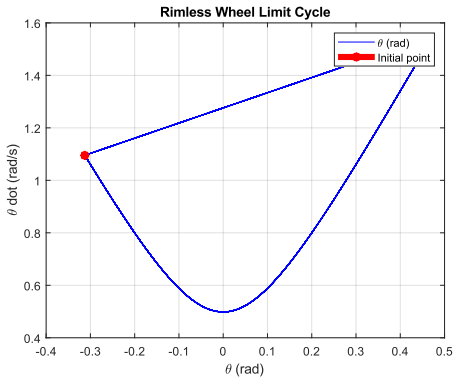

Figura 16: Phase portrait for $\dot{\theta}_0 = 1.095$. The curve closes in a limit cycle, confirming locomotion stability.

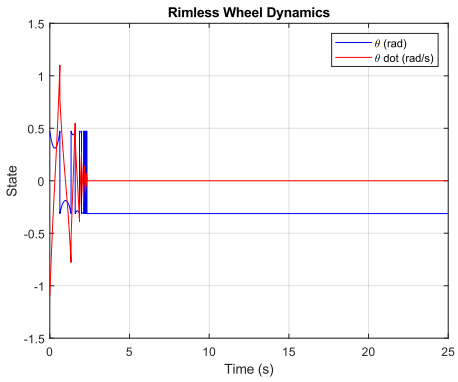

Figura 17: Time evolution for $\dot{\theta}_0 = -1.1$. The system stops quickly due to the braking effect of the slope.

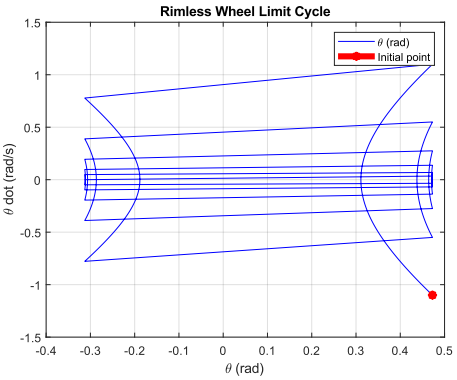

Figura 18: Phase portrait for $\dot{\theta}_0 = -1.1$. No limit cycle: the motion converges to the origin, showing the asymmetry introduced by the slope.

Conclusion The system exhibits a two-phase behavior:

- For **low initial velocities** ($|\dot{\theta}_0| < \dot{\theta}_{critical}$), the wheel stops $\Rightarrow$ *no limit cycle*;
- For **sufficient initial velocities**, the system always converges to a *unique stable limit cycle*.

This behavior confirms the existence of a **basin of attraction** associated with the limit cycle, bounded by initial conditions lacking sufficient energy. The result is consistent with passive walking theory: cyclic motion is self-sustaining only when the tangential component of gravitational force along the slope is able to compensate for energy losses due to impacts.

Question B: The effect of variation of three fundamental physical parameters of the rimless wheel model was analyzed, keeping the initial angular velocity constant at $\dot{\theta}_0 = 0{,}95$ rad/s. The modified parameters are:

- leg length l;
- angle between legs α;
- slope inclination γ.

The goal is to evaluate how such modifications influence dynamic equilibrium conditions and the existence of the limit cycle, by observing the temporal evolution of the states and the phase portrait.

Case 1: Shorter leg – $l = 0{,}8$ m, $\alpha = \pi/8$, $\gamma = 0{,}08$ rad

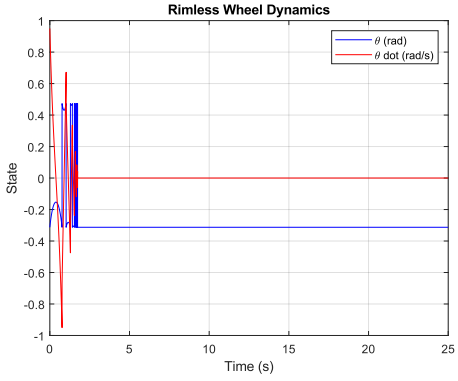

Figura 19: State time evolution for $l = 0.8$ m. The system quickly stops after a few impacts: angular velocity nullifies and cyclic motion is not maintained.

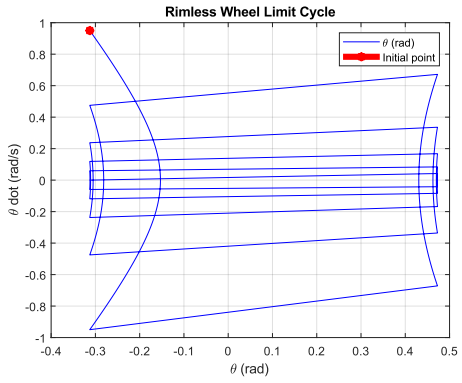

Figura 20: Phase portrait for $l = 0.8$ m. The trajectory converges to the origin, indicating the absence of a stable limit cycle.

The system stops after a few impacts: angular velocity drops to zero and the state converges to a static equilibrium configuration. The shorter leg reduces the center of mass height and thus the

available potential energy, making effective conversion into kinetic energy more difficult. The phase portrait clearly shows the trajectory converging to the origin.

In practice: shortening the leg penalizes dynamics and prevents the maintenance of cyclic motion.

Case 2: Increased angle between legs – $l = 1{,}0$ m, $\alpha = \pi/6$, $\gamma = 0{,}08$ rad

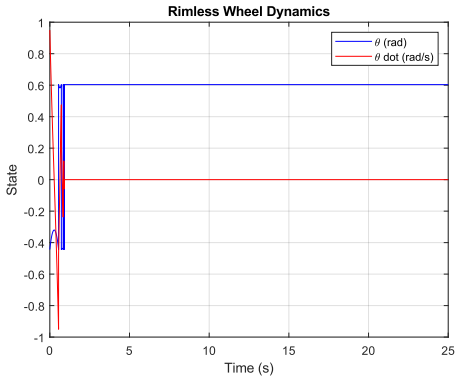

Figura 21: State time evolution for $\alpha = \pi/6$. The system fails to sustain cyclic motion and stops after a few impacts.

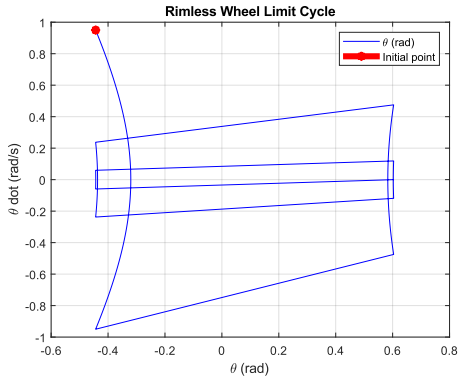

Figura 22: Phase portrait for $\alpha = \pi/6$. The energy loss due to wider impacts causes convergence to equilibrium.

Also in this case, [figure 21] shows the system stopping early. Increasing the angle between the legs increases the distance between successive impact points, causing greater energy losses at each impact. As a result, the energy provided by the slope is no longer sufficient to compensate for these losses. The phase portrait shows a trajectory that collapses to the origin after the first cycle.

In practice: increasing α severely impairs motion conservation.

Case 3: Increased slope inclination – $l = 1{,}0$ m, $\alpha = \pi/8$, $\gamma = 0{,}12$ rad

In this case, the system behaves completely differently: a stable and rapid convergence to a limit cycle is observed. The increased slope inclination provides a stronger gravitational contribution, increasing the available downhill energy. This energy is sufficient to compensate for the impact losses, allowing for sustained motion and a closed stable orbit in the phase portrait.

In practice: a steeper incline favors the maintenance of cyclic locomotion

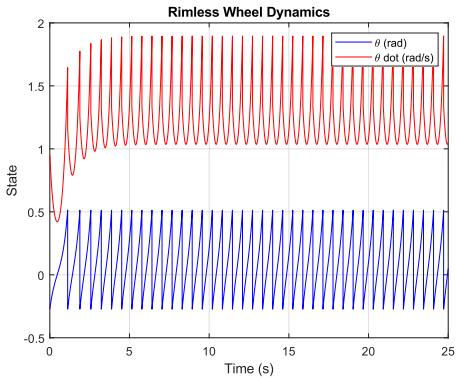

Figura 23: State time evolution for $\gamma = 0.12$ rad. The system shows stable and sustained cyclic oscillation.

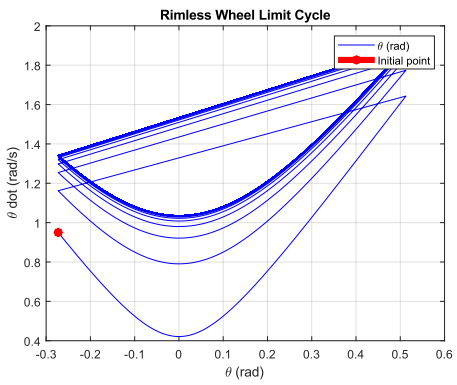

Figura 24: Phase portrait for $\gamma = 0.12$ rad. The system converges to a stable limit cycle, visible as a closed curve.

In practice: a steeper incline favors the maintenance of cyclic locomotion.

Equilibrium conditions are strongly influenced by leg length (l), inter-leg angle (α), and slope inclination (γ). In particular:

- A larger α increases impact losses $\rightarrow$ worsens stability.
- A smaller l lowers the center of mass height $\rightarrow$ limits available potential energy.
- A larger γ provides more gravitational energy $\rightarrow$ improves ability to maintain motion.

The first two cases (short leg and large angle) completely eliminated the limit cycle: the system stopped. The third case (steep slope) resulted in a wider and more stable limit cycle than the standard case, showing more energetic dynamics.

Conclusion

The rimless wheel system is highly sensitive to geometric and environmental parameters. The limit cycle exists only if energy conditions are balanced: gravity must provide enough energy to compensate for impact losses. The analysis shows that a steeper slope favors motion, while overly wide angles or short legs prevent its maintenance.